Cell Stem Cell, Volume xx

Supplemental Information

Hematopoietic Stem Cell-Engineered Invariant Natural Killer T Cell Therapy for Cancer

Yanni Zhu, Drake J. Smith, Yang Zhou, Yan-Ruide Li, Jiaji Yu, Derek Lee, Yu-Chen Wang, Stefano Di Biase, Xi Wang, Christian Hardoy, Josh Ku, Tasha Tsao, Levina J. Lin, Alexander T. Pham, Heesung Moon, Jami McLaughlin, Donghui Cheng, Roger P. Hollis, Beatriz Campo-Fernandez, Fabrizia Urbinati, Liu Wei, Larry Pang, Valerie Rezek, Beata Berent-Maoz, Mignonette Macabali, David Gjertson, Xiaoyan Wang, Zoran Galic, Scott G. Kitchen, Dong Sung An, Siwen Hu-Lieskova, Paula J. Kaplan-Lefko, Satiro N. De Oliveira, Christopher S. Seet, Sarah M. Larson, Stephen J. Forman, James R. Heath, Jerome A. Zack, Gay M. Crooks, Caius G. Radu, Antoni Ribas, Donald B. Kohn, Owen N. Witte, and Lili Yang

A

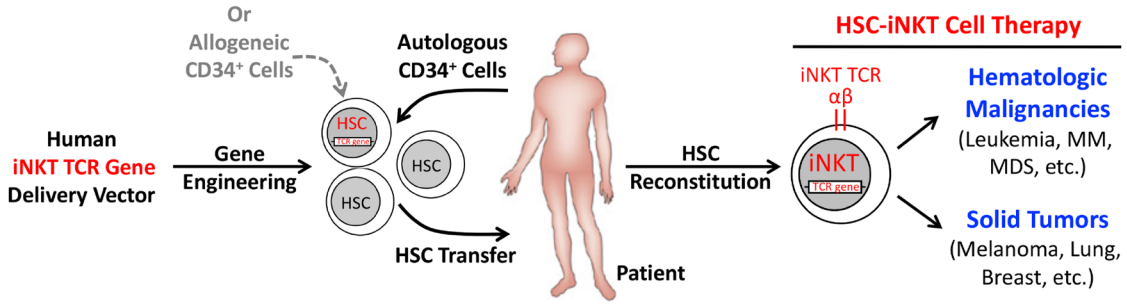

B

Vector Titer (Lenti/iNKT-sr39TK)			
Titer (TU/ml)	**Average**	**STDEV**	**%CV**
Un-Concentrated Supernatant (4 L)	8.27×10^5	6.40×10^4	7.73%
Concentrated Supernatant (2000x fold; 2 ml)	5.30×10^9	2.55×10^8	4.90%

C

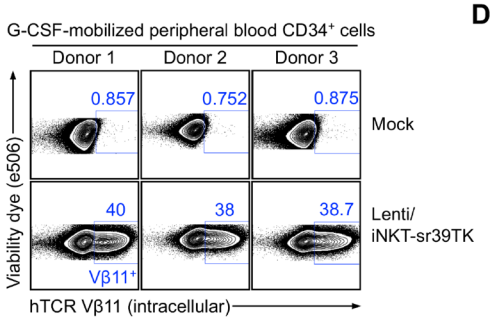

D

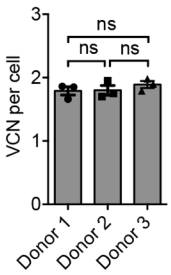

E

Transduction of G-CSF mobilized CD34+ HSCs (1 x 10^6)				
Lenti/iNKT-sr39TK (TU)	0	1 x 10^8	2 x 10^8	4 x 10^8
% Vβ11+	0	19%	39%	51%
VCN	0	1.28	1.73	1.98

Figure S1. Development of a Hematopoietic Stem Cell-Engineered Invariant Natural Killer T (HSC-iNKT) Cell Therapy, Related to Figure 1.

(A) Schematic representation of the concept of HSC-iNKT cell therapy. Autologous or allogeneic human CD34+ HSCs will be collected and engineered *in vitro* with a human iNKT TCR gene, followed by adoptive transfer into cancer patients. Post-HSC reconstitution, iNKT TCR gene-engineered HSCs will continuously produce human iNKT cells. This therapy has the potential to provide cancer patients with therapeutic levels of iNKT cells for a lifetime. HSC-iNKT cell therapy may benefit patients with a broad range of cancers, including various hematologic malignancies and solid tumors. MM, multiple myeloma; MDS, myelodysplastic syndromes.

(B) Titer of the Lenti/iNKT-sr39TK vector. A 4-liter batch of Lenti/iNKT-sr39TK lentiviral vector was produced using a 293T virus packaging cell line transient transfection method, followed by concentration to 2 ml (2000x fold) using an established tandem tangential filtration method. Vector titers prior to and post-concentration were measured by transducing HT29 cells with serial dilutions and performing digital QPCR (n = 3). TU, transduction unit.

(C-D) Transduction of HSCs with the Lenti/iNKT-sr39TK vector. G-CSF-mobilized peripheral blood CD34+ HSCs from three healthy donors were studied. Concentrated Lenti/iNKT-sr39TK vector were added to HSC cultures (2 x 10^8 TU per 1 x 10^6 HSCs). Three days later, a portion of HSCs were collected and analyzed for intracellular expression of iNKT TCR (identified as hTCR

Vβ11$^+$) using flow cytometry (C). 14 days later, the remaining HSCs were collected and analyzed for average vector copy number (VCN) per cell using droplet digital PCR (ddPCR) (D; n = 3).

(E) Titrated transduction of HSCs with the Lenti/iNKT-sr39TK vector. Representative data studying G-CSF-mobilized peripheral blood CD34$^+$ HSCs from a selected donor were presented. Titrated amount of concentrated Lenti/iNKT-sr39TK vector were added to HSC cultures. Three days later, a portion of HSCs were collected and analyzed for intracellular expression of iNKT TCR (identified as hTCR Vβ11$^+$) using flow cytometry. 14 days later, the remaining HSCs were collected and analyzed for average VCN per cell using ddPCR. Note the correlation between vector titers and transduction rates. Average VCN per cell at all transduction rates remained between 1-3, which is considered to be a relative safe range for lentivector-mediated gene therapy.

Representative of 2 experiments. Data were presented as the mean ± SEM. ns, not significant, by 1-way ANOVA (D).

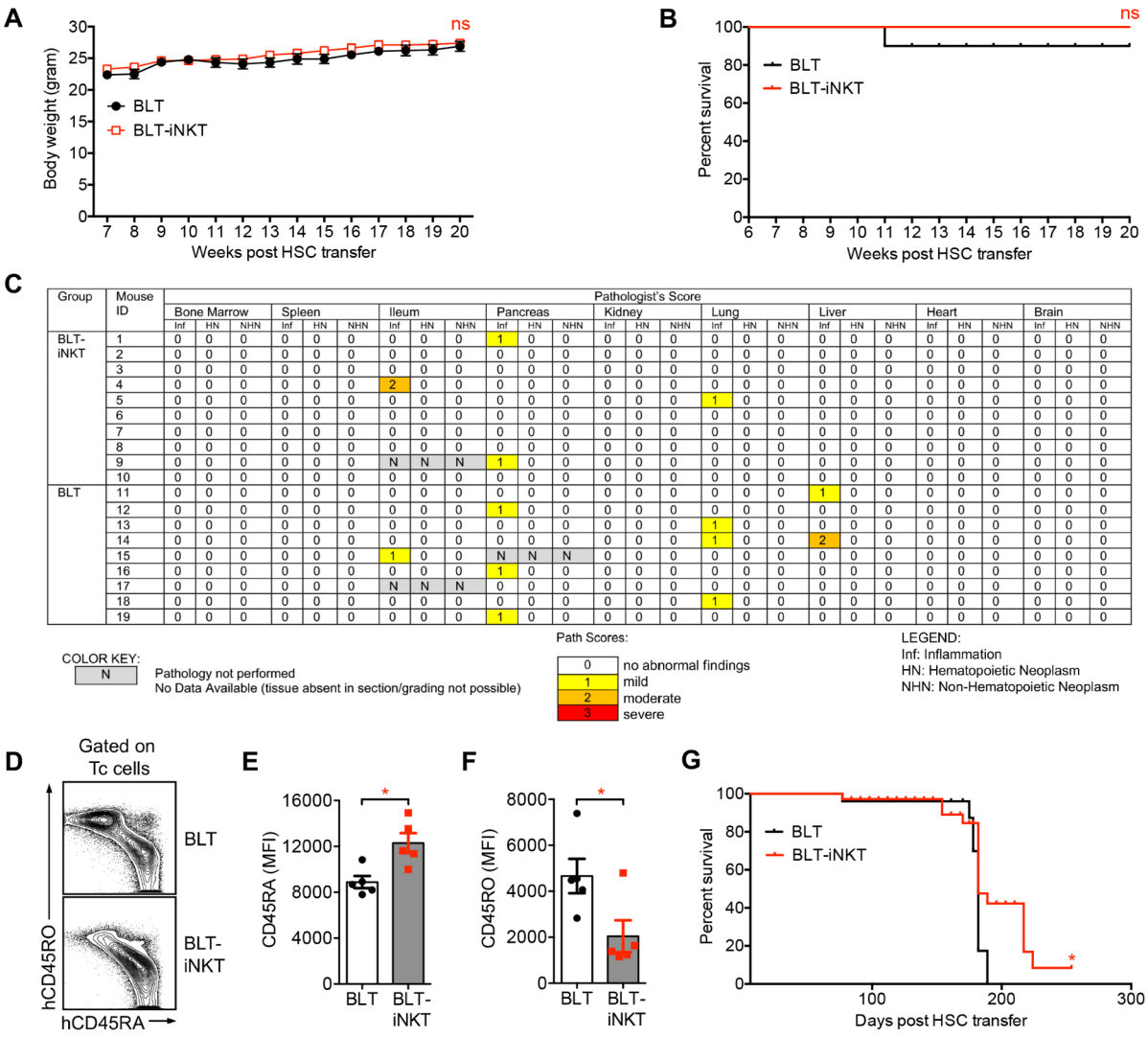

Figure S2. Safety Study of HSC-iNKT Cell Therapy in BLT-iNKT Humanized Mice, Related to Figure 3.

Representative data were presented, studying BLT-iNKT mice produced with human fetal thymus and Lenti/iNKT-sr39TK vector-transduced PBSCs. BLT mice generated in parallel using the same fetal thymus and PBSCs (mock-transduced) were included as a control.

(A-C) Monitoring of BLT-iNKT mice and control BLT mice over a period of 5 months post-HSC transfer, followed by tissue collection and pathological analysis. (A) Mouse body weight (n = 9-10). (B) Kaplan-Meier analysis of mouse survival rate (n = 9-10). (C) Mouse pathology. Various tissues were collected and analyzed by the UCLA Pathology Core. Tissues were analyzed for inflammation (Inf), hematopoietic neoplasm (HN), and non-hematopoietic neoplasm (NHN). Data were presented as pathologist's scores of individual mouse tissues (n = 9-10). 0, no abnormal findings; 1, mild; 2, moderate; 3, severe.

(D-F) Analysis of the auto-activation of human conventional T cells in BLT-iNKT and control BLT mice at 6 months post-HSC transfer. (D) FACS plots showing the expression of CD45RA and CD45RO markers on human T cells isolated from the liver of experimental mice. Tc, human

conventional αβ T cells (gated as $hCD45^+hTCR\alpha\beta^+6B11^-$ cells). (E-F) Quantification of D (n = 5). Note that compared to Tc cells isolated from the control BLT mice, Tc cells isolated from the BLT-iNKT mice displayed a less antigen-experienced phenotype (marked as $hCD45RA^{lo}hCD45RO^{hi}$), indicating their reduced graft-versus-host (GvH) responses in BLT-iNKT mice.

(G) Kaplan-Meier survival curves of BLT-iNKT mice and control BLT mice over a period of 8 months post-HSC transfer. N = 14-19. Mice were combined from 2 independent experiments.

Representative of 2 experiments. Data are presented as the mean ± SEM. ns, not significant, *P < 0.05, by Student's *t* test (A, E, F) or by log rank (Mantel-Cox) test adjusted for multiple comparisons (B, G).

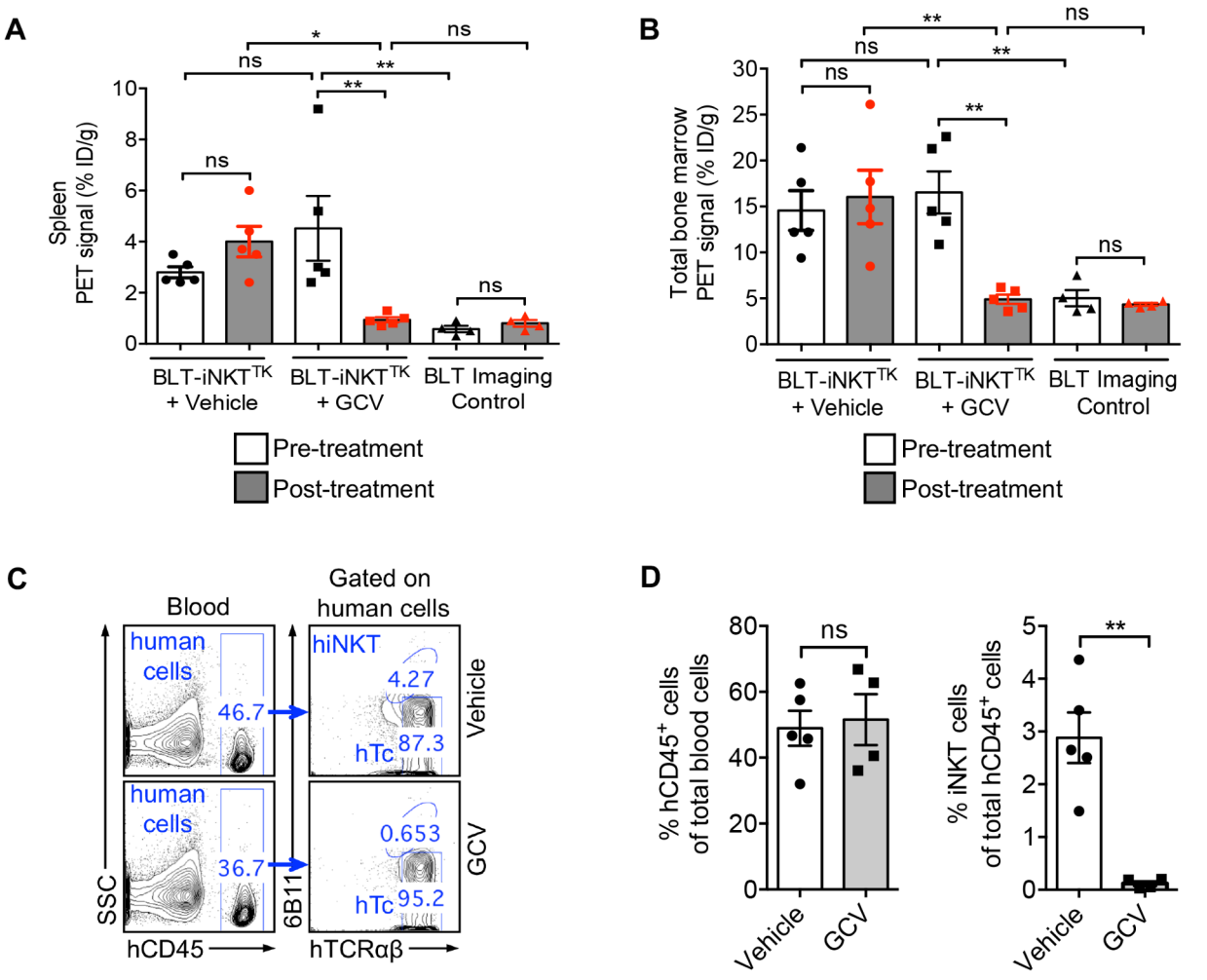

Figure S3. Controlled Depletion of HSC-iNKT Cells in BLT-iNKT Humanized Mice, Related to Figure 3.

Representative data were presented, studying BLT-iNKT^{TK} mice produced with human fetal thymus and Lenti/iNKT-sr39TK vector-transduced PBSCs. BLT mice generated in parallel using the same fetal thymus and PBSCs (mock-transduced) were included as a control.

(A) Statistical analysis of PET/CT signals in the spleen of BLT-iNKT^{TK} and control BLT mice pre- and post-GCV treatment (n= 4-5).

(B) Statistical analysis of PET/CT signals in the bone marrow of BLT-iNKT^{TK} and control BLT mice pre- and post-GCV treatment (n = 4-5).

(C-D) FACS validation of controlled depletion of HSC-engineered human iNKT (HSC-iNKT) cells in BLT-iNKT^{TK} mice via GCV treatment. (C) Representative FACS plots of blood cells. (D) Quantification of C (n= 4-5). Note the selective depletion of HSC-iNKT cells (gated as hCD45^{+} hTCR$\alpha\beta^{+}$6B11^{+} cells) but not the overall human immune cells (gated as total hCD45^{+} cells) in BLT-iNKT^{TK} mice post-GCV treatment.

Representative of 2 experiments. Data are presented as the mean ± SEM. ns, not significant, *P < 0.05, **P < 0.01, by 1-way ANOVA (A, B) or by Student's *t* test (D).

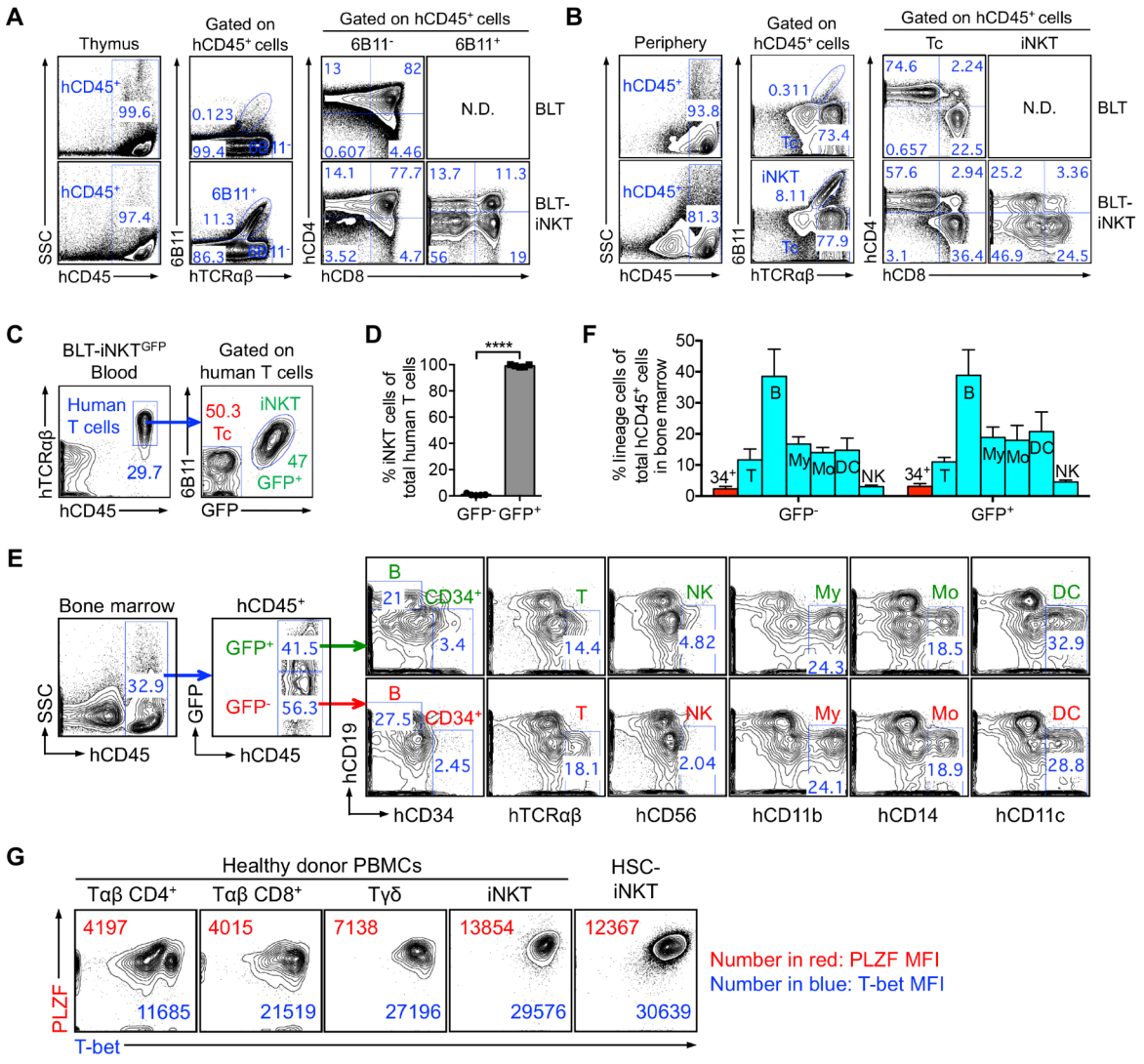

Figure S4. Development, Phenotype, and Functionality of HSC-iNKT Cells; Related to Figure 4.

Representative data were presented, studying HSC-iNKT cells generated from BLT-iNKT mice produced with Lenti/iNKT-sr39TK vector (A-B, G) or Lenti/iNKT-EGFP vector (C-F) transduced PBSCs.

(A) FACS plots showing the analysis of cells isolated from the human thymus implants of BLT-iNKT mice and control BLT mice. Note the detection of developing HSC-iNKT cells (gated as $hCD45^+hTCR\alpha\beta^+6B11^+$) in BLT-iNKT mice but not in control BLT mice. N.D., not detected.

(B) FACS plots showing the analysis of cells isolated from the periphery (blood) of BLT-iNKT mice and of control BLT mice. Note the detection of mature HSC-iNKT cells (gated as $hCD45^+hTCR\alpha\beta^+6B11^+$) in BLT-iNKT mice but not in control BLT mice. N.D., not detected.

(C-F) Lineage commitment of iNKT TCR gene-engineered human HSCs. BLT-iNKT mice generated with Lenti/iNKT-EGFP vector-transduced PBSCs were studied (denoted as BLT-iNKT^{GFP} mice). (C) FACS plots showing the analysis of human $\alpha\beta$ T cells (pre-gated as hTCR45$^+$hTCR$\alpha\beta^+$ cells) present in the blood of BLT-iNKT^{GFP} mice, studying the correlation of GFP expression and iNKT cell (gated as 6B11$^+$) commitment. (D) Quantification of C (n = 5). (E) FACS plots showing the analysis of bone marrow cells of BLT-iNKT^{GFP} mice. (F) Quantification of E, showing the quantification of various lineages of human immune cells within the GFP$^-$ and GFP$^+$ subpopulations (pre-gated as hCD45$^+$GFP$^-$ and hCD45$^+$GFP$^+$, respectively) (n = 5). CD34$^+$ (34$^+$), CD34$^+$ hematopoietic stem and progenitor cells (gated as Lin$^-$hCD34$^+$); T, T cells (gated as hTCR$\alpha\beta^+$); B, B cells (gated as hCD19$^+$); My, myeloid cells (gated as hCD11b$^+$); Mo, monocytes/macrophages (gated as hCD14$^+$); DC, dendritic cells (gated as hCD11c$^+$); NK, natural killer cells (gated as hCD56$^+$).

(G) FACS plots showing the intracellular expression of master transcription factors PLZF and T-bet in HSC-iNKT cells. Various lineages of native human T cells isolated from healthy donor peripheral blood were studied as controls, including iNKT cells (identified as hTCR$\alpha\beta^+$6B11$^+$ cells), conventional CD4$^+$ $\alpha\beta$ T cells (T$\alpha\beta$ CD4$^+$; identified as hTCR$\alpha\beta^+$6B11$^-$CD4$^+$CD8$^-$ cells), conventional CD8$^+$ $\alpha\beta$ T cells (T$\alpha\beta$ CD4$^+$; identified as hTCR$\alpha\beta^+$6B11$^-$CD4$^-$CD8$^+$ cells), and gamma-delta T cells (T$\gamma\delta$; identified as hTCR$\gamma\delta^+$ cells).

Representative of 2 experiments. Data were presented as the mean ± SEM. ****P < 0.0001, by Student's *t* test.

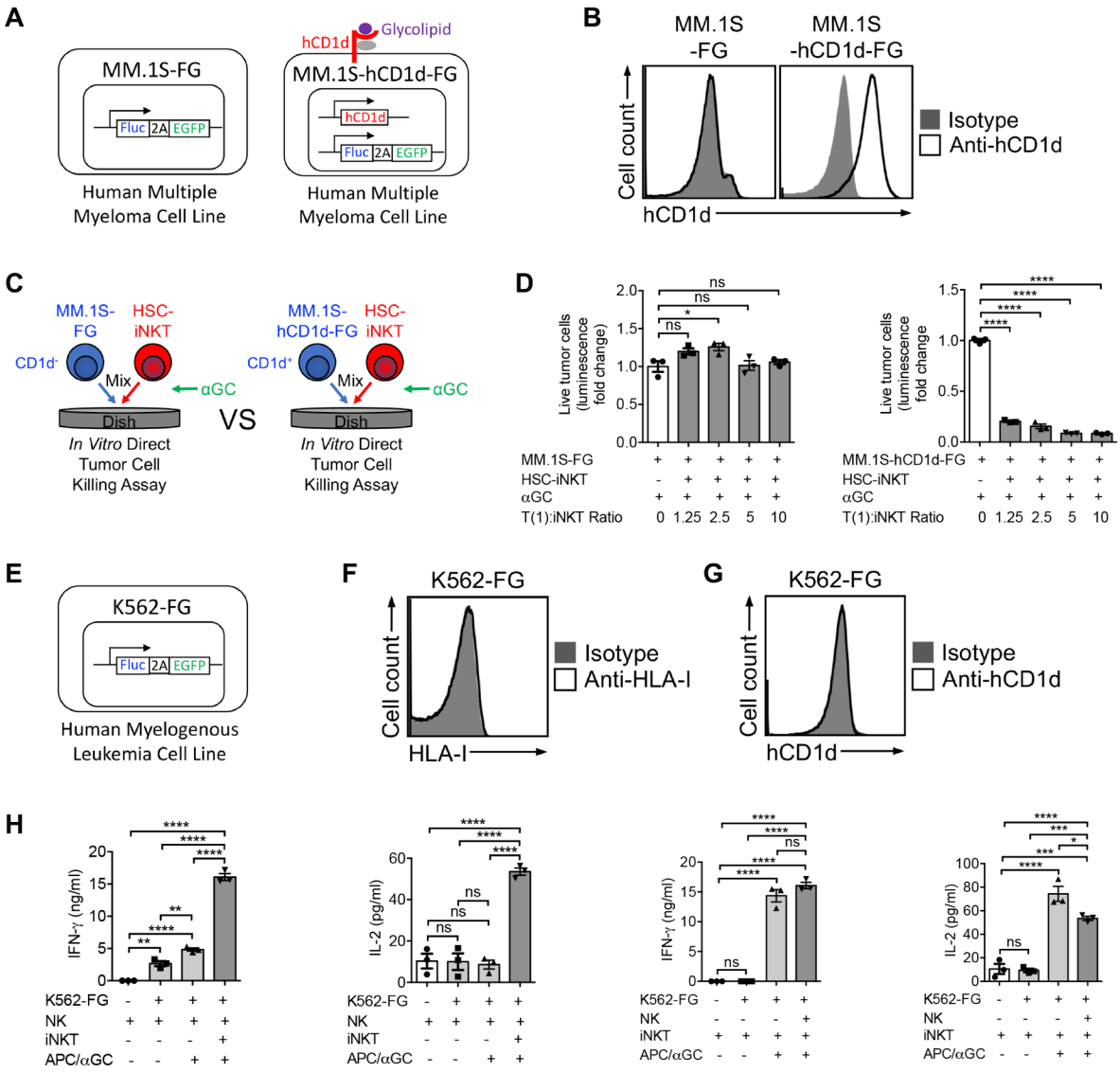

Figure S5. Tumor-Attacking Mechanisms of HSC-iNKT Cells: Direct Killing of CD1d$^+$ Tumor Cells and NK Adjuvant Effects, Related to Figure 5, B-I.

(A-D) Schematics showing the engineered MM.1S-FG and MM.1S-hCD1d-FG cell lines. MM.1S is a human multiple myeloma cell line. MM.1S-FG cell line was generated by stably transducing the parental MM.1S cell line with a Lenti/FG lentiviral vector encoding a firefly luciferase (Fluc) reporter gene and an enhanced green fluorescent protein (EGFP) reporter gene. MM.1S-hCD1d-FG cell line was generated by stably transducing the MM.1S-FG cell line with another Lenti/CD1d lentiviral vector encoding the human CD1d gene.

(B) FACS plots showing the detection of CD1d on MM.1S-hCD1d-FG cells, but not on MM.1S-FG cells.

(C-D) Studying the CD1d/αGC-mediated killing of tumor cells by HSC-iNKT cells. (C) Experimental design. (D) Tumor killing data from C (n = 3). Note the aggressive killing of tumor cells in a CD1d-dependant manner in the presence of αGC.

(E) Schematic of the K562-FG cell line. K562 is a human myelogenous leukemia cell line that is sensitive to NK cell-mediated tumor killing. The K562-FG cell line was generated by stably transducing the parental K562 cell line with a Lenti/FG lentiviral vector encoding Fluc and EGFP dual reporter genes.

(F) FACS plot showing the absence of MHC class I (HLA-I) expression on K562-FG cells.

(G) FACS plot showing the absence of CD1d expression on K562-FG cells.

(H) ELISA analysis of IFN-γ and IL-2 in the supernatants of various mixed cell cultures (tumor:NK:iNKT ratio 1:2:2), showing the massive production of these cytokines by HSC-iNKT cells post-APC/αGC stimulation (n = 3).

Representative of 2 experiments. Data were presented as the mean $\pm$ SEM. ns, not significant, *P < 0.05, **, P<0.01, ***P < 0.001, ****P < 0.0001, by 1-way ANOVA.

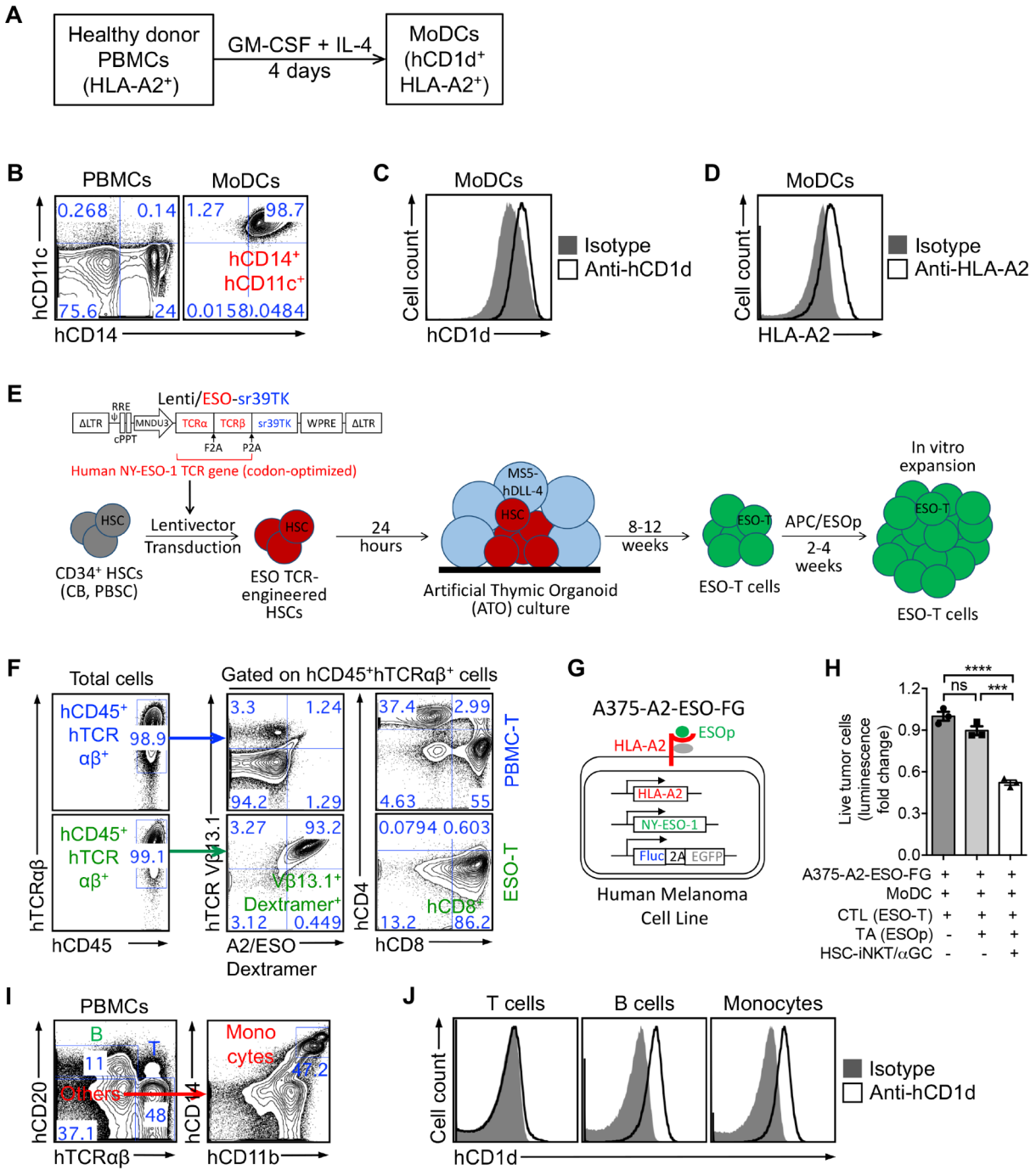

Figure S6. Tumor-Attacking Mechanisms of HSC-iNKT Cells: Adjuvant Effects of HSC-iNKT Cells on Boosting DC/CTL Antitumor Reactions and Inhibiting TAMs, Related to Figure 5, J-S.

(A) Diagram showing the experimental design to generate HLA-A2$^+$hCD1d$^+$ human MoDCs. PBMCs, peripheral blood mononuclear cells; MoDCs, monocyte-derived dendritic cells.

(B) FACS plots showing the lineage verification of MoDCs (identified as $hCD14^+hCD11c^+$). PBMCs were included as a staining control.

(C) FACS plot showing the detection of CD1d on MoDCs.

(D) FACS plot showing the detection of HLA-A2 on MoDCs.

(E) Diagram showing the experimental design to generate NY-ESO-1-specific human CD8 cytotoxic T lymphocytes (denoted as ESO-T cells). Human $CD34^+$ HSCs were transduced with a Lenti/ESO-sr39TK vector, then differentiated into ESO-T cells in an artificial thymic organoid (ATO) culture, following by *in vitro* expansion of ESO-T cells with APC/ESOp stimulation. Human $CD34^+$ HSCs were isolated from cord blood (CB) or G-CSF-mobilized peripheral blood (denoted as peripheral blood stem cells, PBSCs). Lenti/ESO-sr39TK, lentivector encoding a human NY-ESO-1 TCR gene as well as an sr39TK suicide/PET imaging reporter gene; MS5-hDLL4, MS5 murine bone marrow stromal cell line engineered to express human Delta Like Canonical Notch Ligand 4; APC/ESOp, antigen-presenting cell (irradiated $HLA\text{-}A2^+$ healthy donor PBMCs) loaded with NY-ESO-$1_{157\text{-}165}$ peptide (ESOp). The transgenic NY-ESO-1 TCR recognizes NY-ESO-1 peptide presented by HLA-A2.1, and comprises a $V\beta\ 13.1^+$ beta chain.

(F) FACS plots showing the phenotype of ESO-T cells (characterized as $hCD45^+hTCR\alpha\beta^+hTCR\ V\beta13.1^+A2/ESO\ Dextramer^+hCD4^-hCD8^+$). Human T cells expanded from healthy donor PBMCs through anti-CD3/CD28 Dynabeads stimulation were included as a staining control (denoted as PBMC-T cells). HLA-A2.1/NY-ESO-$1_{157\text{-}165}$ (A2/ESO) dextramer is a FACS staining reagent that detects HLA-A2.1-restricted and NY-ESO-1-specific human TCRs.

(G) Schematic showing the engineered A375-A2-ESO-FG cell line. A375 is a human melanoma cell line. A375-A2-ESO-FG cell line was generated by stably transducing the parental A375 cell line with lentivectors encoding an HLA-A2.1 gene, a NY-ESO-1 gene, and the Fluc and EGFP dual reporter genes.

(H) Tumor killing by ESO-T cells (n = 3). ESO-T cells were stimulated with MoDC/ESOp in the presence or absence of HSC-iNKT/αGC, followed by co-culture with A375-A2-ESO-FG tumor cells and analysis of tumor killing (tumor:DC:CTL:iNKT ratio 1:1:1:0.5).

(I) FACS plots showing the identification of T cells (gated as $hTCR\alpha\beta^+$ cells), B cells (gated as $hCD20^+$ cells), and monocytes (gated as $hCD14^+$ cells) from healthy donor peripheral blood mononuclear cells (PBMCs).

(J) FACS plots showing the measurement of CD1d expression on PBMC T cells, B cells, and monocytes gated from A. Note CD1d was highly expressed on antigen presenting cells (APCs) like B cells and monocytes, but not on T cells.

Representative of 2 experiments. Data were presented as the mean $\pm$ SEM. ns, not significant, ***P < 0.001, ****P < 0.0001, by 1-way ANOVA (H).

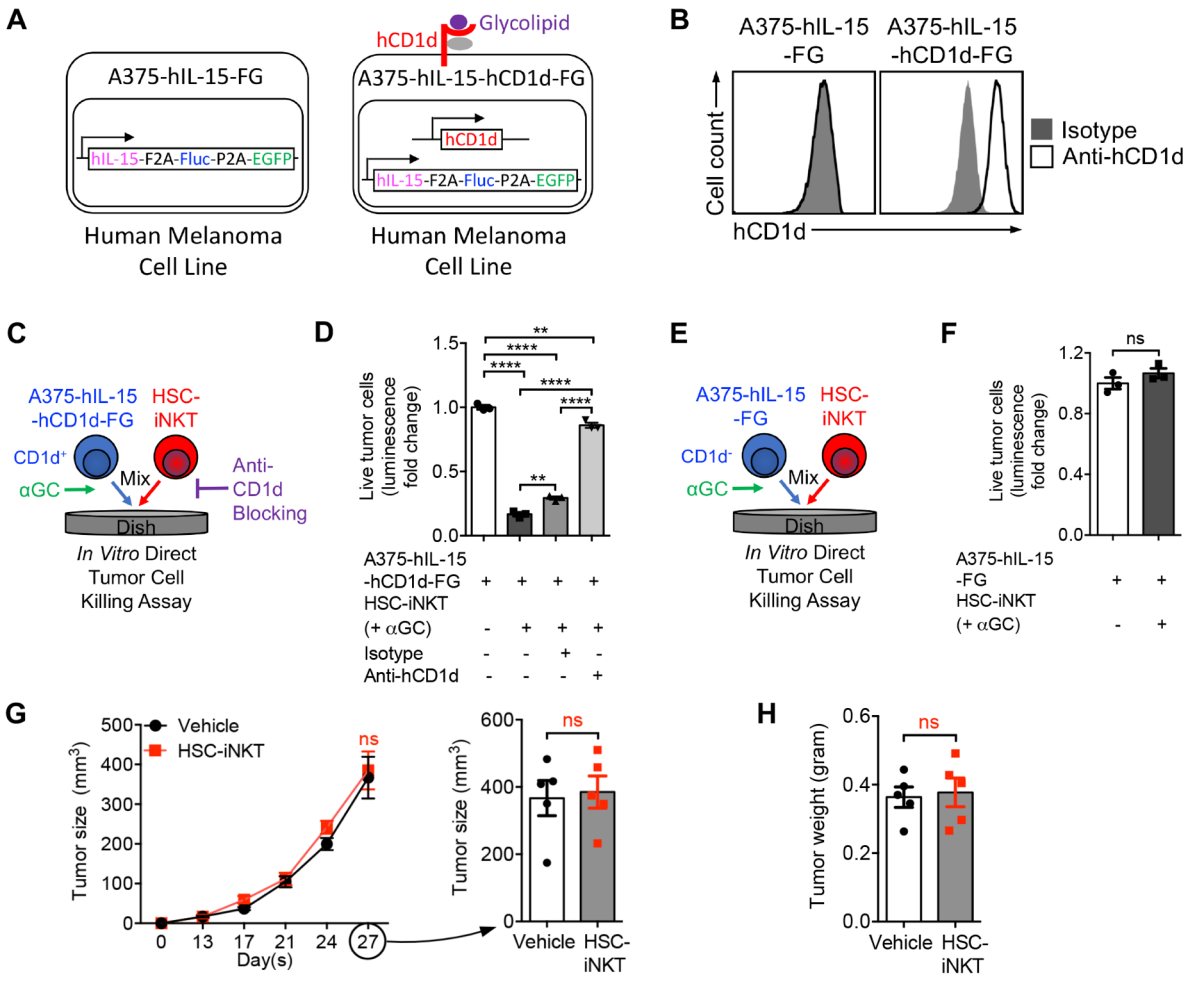

Figure S7. *In Vivo* Antitumor Efficacy of HSC-iNKT Cells Against Solid Tumors in a Human Melanoma Xenograft Mouse Model, Related to Figure 7.

(A) Schematics showing the engineered A375-hIL-15-FG and A375-hIL-15-hCD1d-FG cell lines. A375 is a human melanoma cell line. A375-hIL-15-FG cell line was engineered by stably transducing the parental A375 cell line with a Lenti/hIL-15-FG lentiviral vector encoding a human IL-15 gene, a Fluc reporter gene, and an EGFP reporter gene. A375-hIL-15-hCD1d-FG cell line was generated by stably transducing the A375-hIL-15-FG cell line with a Lenti/CD1d lentiviral vector encoding the human CD1d gene.

(B) FACS plots showing the detection of CD1d on A375-hIL-15-hCD1d-FG cells, but not on A375-hIL-15-FG cells.

(C-D) Studying the *in vitro* direct killing of A375-hIL-15-hCD1d-FG cells by HSC-iNKT cells in the presence of αGC (tumor:iNKT ratio 1:2). (C) Experimental design. (D) Tumor killing (n = 3). Note that tumor killing was dependent on CD1d.

(E-F) Studying the *in vitro* direct killing of A375-hIL-15-FG cells by HSC-iNKT cells in the presence of αGC (tumor:iNKT ratio 1:2). (E) Experimental design. (F) Tumor killing (n = 3). Note the lack of tumor killing in the absence of CD1d.

(G-H) Studying the *in vivo* antitumor efficacy of HSC-iNKT cells in the control A375-hIL-15-FG human melanoma xenograft NSG mouse model (related to main Figures 7J-7L). (G) Measurements of tumor size over time (n = 5). (H) Measurements of tumor weight at the terminal harvest on day 28 (n = 5).

Representative of 2 experiments. Data were presented as the mean ± SEM. ns, not significant, **P < 0.01, ****P < 0.0001, by 1-way ANOVA (D) or by Student's *t* test (F, G, H).